International Journal of Minerals, Metallurgy and Materials
Volume 26, Number 6, June 2019, Page 681
https://doi.org/10.1007/s12613-019-1782-0

Carbon and oxygen behavior in the RH degasser with carbon powder addition

Jian-long Guo[1)], *Li-hua Zhao*[2)], *Yan-ping Bao*[1)], *Shuai Gao*[1)], *and Min Wang*[1)]

1) State Key Laboratory of Advanced Metallurgy, University of Science and Technology Beijing, Beijing 100083, China
2) School of Metallurgical and Ecological Engineering, University of Science and Technology Beijing, Beijing 100083, China
(Received: 3 December 2018; revised: 12 January 2019; accepted: 22 January 2019)

Abstract: For ultra-low-carbon (ULC) steel production, the higher oxygen content before Ruhrstahl-Heraeus (RH) decarburization (de-C) treatment could shorten the de-C time in the RH degasser. However, this would lead to oxidation rates being exceeded by molten steel production, affecting ULC steel surface quality. In this work, a carbon powder addition (CPA) process was proposed to reduce the dissolved oxygen content at the end of RH de-C through addition of carbon powder to molten steel in the vacuum vessel. Carbon and oxygen behavior during the CPA and conventional process was then studied. The results demonstrated that the de-C rate with CPA was lower compared to the conventional process, but the carbon content at the end of de-C presented no difference. The de-C reaction for CPA process took place in the four reaction sites: (1) within the bulk steel where the spontaneous CO bubbles form; (2) splashing area on the liquid steel surface; (3) Ar bubble surface; (4) molten steel surface. The CPA process could significantly reduce the dissolved oxygen content at the end of de-C, the sum content of FeO and MnO in the slag, the aluminum consumption, and the defect rate of rolled products. This was beneficial in improving ULC steel cleanliness.

Keywords: ultra-low-carbon steel; ruhrstahl-Heraeus degasser; carbon powder; de-C; pre-deoxidization

1. Introduction

The Ruhrstahl-Heraeus (RH) is a widely utilized vacuum device in secondary refining, involving many metallurgical functions, such as decarburization (de-C), deoxidization, degassing, desulfurization, inclusion removal, and alloying [1–3]. The content of carbon in liquid steel ([C]) should be below 15×10^{-6} to ensure cold-rolled sheet formability. In addition, the content of dissolved oxygen in liquid steel ($[O]_D$) at the end of de-C should be controlled to ensure the surface-quality requirements of the cold-rolled sheet [4–6]. Consequently, a major problem in the production of ultra-low-carbon (ULC) steel is the coordinated control of carbon and oxygen in the liquid steel.

Many studies have been conducted to understand these problems. In most cases, the increasing liquid-steel circulation rate could decrease both the de-C time and [C] content, both of which are functions of the parameters of the RH equipment and operation, such as increasing the diameter of snorkels [7], using the oval snorkels [8], using the multi-snorkels [9–10] and increasing the rate of gas-lifting flow [11]. Lower RH slag oxidizability and the reduction in the number of inclusions could effectively improve the surface quality of the cold-rolled sheet [12–14]. Many measures could reduce the number of inclusions, including forced de-C, which reduces the total oxygen (T.O) content in liquid steel during tapping of the converter and end de-C from the RH [5,15–16]. Reasonable converter-end-point control ensures good steel conditions before RH treatment; however, due to the effects of furnace conditions, furnace type, combined blowing, operation parameters, scrap concentration, and raw material, the end point of the converter is not stable.

Fig. 1 shows the relationship between [C] content and $[O]_D$ content before RH de-C treatment in the Magang (Group) Holding Co., Ltd. (Masteel for short), China. In region A, 95% of the heats were sufficient to satisfy the requirement for natural de-C. In region B, all heats used forced de-C. In these two regions, the $[O]_D$ content at the end of de-C could be controlled within 200×10^{-6}–300×10^{-6}. In region C, the higher $[O]_D$ content could shorten the time of

Corresponding author: Li-hua Zhao E-mail: zhaolihua@metall.ustb.edu.cn

de-C in the RH. However, the higher $[O]_D$ amount would lead to excess oxidation of the molten steel, consequently increasing aluminum consumption and Al_2O_3-inclusion amounts, as well as increasing oxidizability in the slag, which adversely affects the cold-rolled sheets surface quality [17–18].

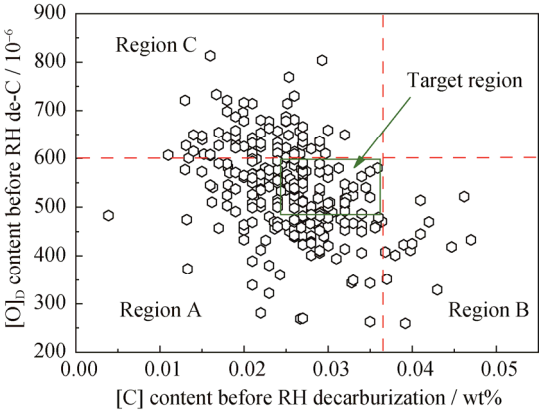

Fig. 1. Relationship between [C] content and $[O]_D$ content prior to RH de-C.

In this paper, a process is proposed to reduce the $[O]_D$ at the end of RH de-C through the addition of carbon powder to the molten steel in the vacuum vessel during RH. The effects of de-C and oxygen behavior following carbon powder addition (CPA) and the conventional process were clarified and compared, and the de-C mechanism for the CPA process was studied. Afterward, industrial trials were conducted to study the effect of CPA on the aluminum consumption and the defect rate of rolled products.

This study is a portion of a large-scale research project, where a CPA pre-deoxidization of the RH process is developed and performed.

2. Materials and methods

2.1. Experimental procedure

The total production route was: Kanbara reactor (KR)→Basic Oxygen Furnace (BOF)→RH→Continuous casting, and the experiments were carried out with the 300 t ladle in the Masteel, during the RH process. The RH equipment parameters are shown in Table 1. The other crucial experimental conditions are shown in Table 2, while the initial compositions are close. The tests were divided into conventional and CPA processe. The production procedures for the two RH processes are shown in Fig. 2. In the CPA process, the addition time of the carbon powder was 3 min subsequent to vacuum, while the added amount was 50 kg. To prevent splashing during the CPA process, the added amount of carbon powder was not more than 20 kg at a time, and the time interval was 30 s.

Table 1. Parameters of RH vacuum degasser

Ladle capacity / t	Vacuum inner diameter / mm	Snorkel inner diameter / mm	Vacuum pumping capacity / ($kg \cdot h^{-1}$)
300	2500	750	1200

Table 2. Various parameters during conventional and CPA process

Process	[C] content / 10^{-6}	$[O]_D$ content / 10^{-6}	Temperature / °C	Carbon powder amount / kg
Conventional process	231	622	1615	—
CPA process	233	630	1611	50

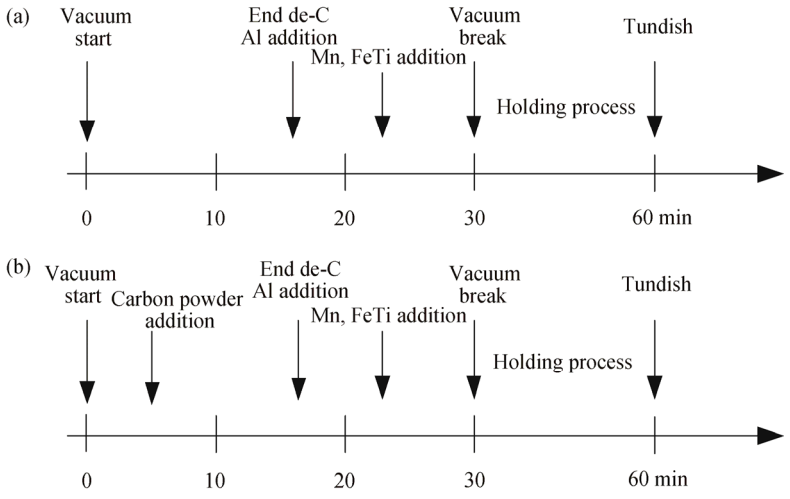

Fig. 2. Diagrammatic scheme of two RH processes: (a) conventional process; (b) CPA process.

2.2. Sampling and analysis

The RH degasser schematic diagram is shown in Fig. 3. The carbon powder was added to the molten steel through an alloy pipe, located at the upper part of the vacuum vessel. The gas evolution during RH process was analyzed and recorded with an infrared gas analysis system. The vacuum pressure variation was observed with the vacuum gauge. Also, the reaction during the CPA was recorded with a video camera installed in the vacuum vessel. Fig. 4 shows the CPA process image, which was recorded with the video camera. The particle size distribution of the carbon powder was 1–5 mm as shown in Fig. 5, of which, 73% were concentrated within 1.5–3.5 mm.

During the de-C reaction, the industrial samples were taken by the ULC sampler every 1–2 min subsequent to the vacuum stored in the ladle near the down-snorkel. Carbon analysis of the samples was conducted through combustion-infrared absorptiometry with an electrical resistance furnace. The real-time changes of the $[O]_D$ content and the temperature of liquid steel were analyzed with a Heraeus oxygen probe. In order to ensure the consistency of the test results, certain process parameters were set to a fixed value,

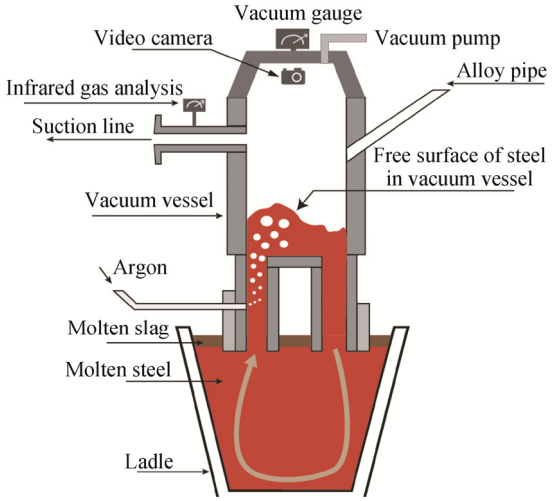

Fig. 3. Schematic of RH degasser for steel refining.

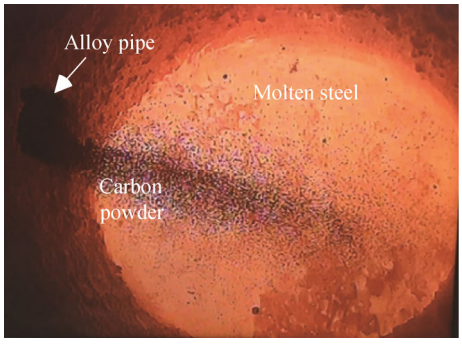

Fig. 4. Industrial test of CPA process in vacuum vessel.

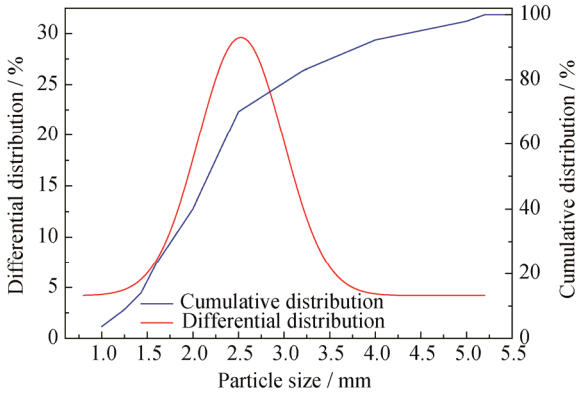

Fig. 5. Distribution curve of carbon powder particle size.

such as Ar flow rate in the upper snorkel, RH vessel dimensions, steel composition entering RH vessel, and snorkels' immersion depth.

3. Results and discussion

3.1. Effect of CPA on de-C in RH process

The [C] content change during RH de-C of the two processes is showed in Fig. 6(a). For conventional process, when the vacuum started at 0 to 4 min, the [C] content dropped quickly to 50×10^{-6}, while the [C] content was reduced to approximately 10×10^{-6} at 15 min. For CPA process, following the powder addition, the [C] content increased, but after approximately 1 min, the [C] content began to decrease abruptly from 100×10^{-6} to 50×10^{-6} within 4 min, while the [C] content fell to 10×10^{-6} at 16 min.

Vacuum pressure and variation of CO concentration are key factors in the de-C rate and could explain the rate change during the de-C reaction [19]. Fig. 6(b) presents the evolution of vacuum pressure in the vacuum vessel. It is clear that, for conventional process, the vacuum level in the RH vessel dropped from 1×10^5 Pa to below 100 Pa quickly and then maintained until the end of RH de-C. For CPA process, the vacuum level coincided with the conventional process level before the CPA. Moreover, with the CPA, the vacuum level increased sharply from 1.8×10^4 to 3.0×10^4 Pa. The main reason for the increased pressure is that a large amount of CO is produced instantly in the CPA process, whereas, due to the strong reaction between $[O]_D$ and C powder in the vacuum vessel, the generated CO exceeded the exhausting capacity of the vacuum pump, which controlled the pressure of the vacuum vessel. The CO concentration variation is shown in Fig. 6(c). For the conventional process, the CO concentration peaked at 4 min. For CPA process, the CO concentration peak was ap-

parently higher and its peak was attained at a slower rate compared to that with the conventional process, indicating that the carbon-oxygen reaction was more intense following the CPA.

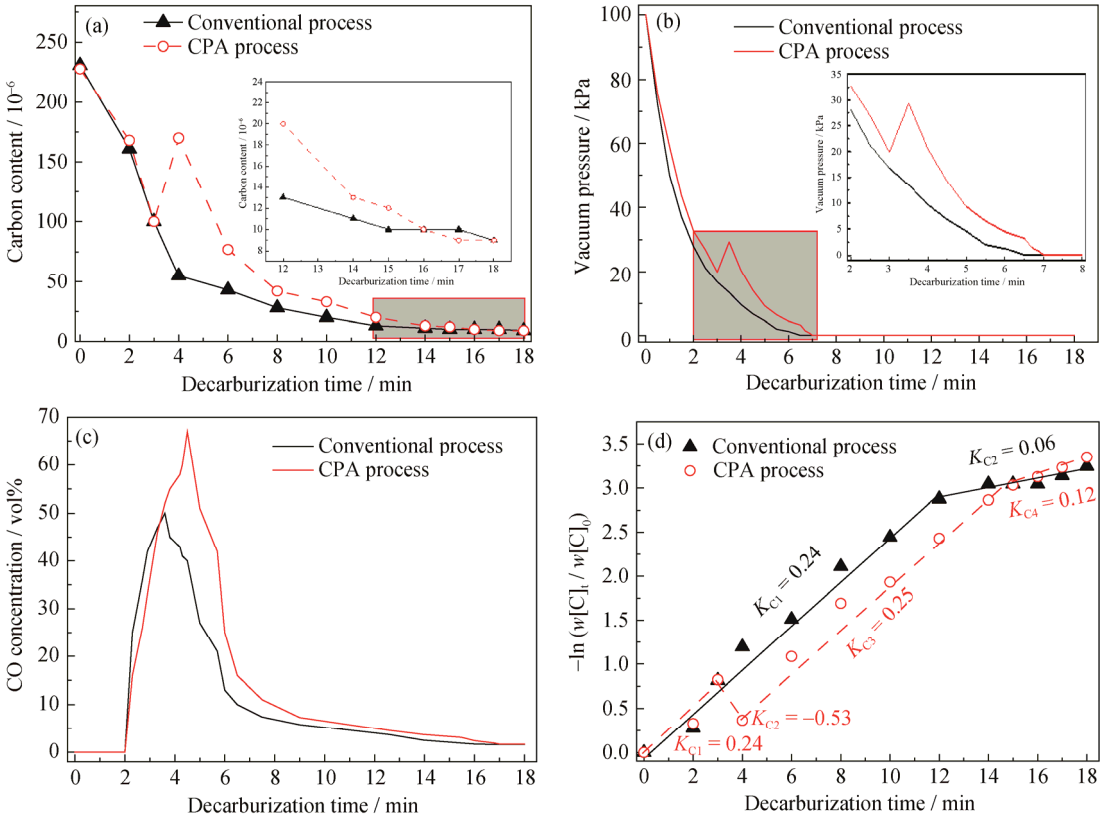

Fig. 6. Changes in [C] content (a), evolution of pressure in the RH vacuum vessel (b), variation of CO concentration (c), and changes in apparent de-C rate constant (d) during RH de-C.

The apparent de-C rate constant, K_C, was regarded as a characteristic parameter of the RH de-C rate [20–21]. Fig. 6(d) shows the K_C change for different processes. The RH de-C was assumed to be a first-order reaction and the K_C was calculated through Eqs. (1) and (2) as follows:

$$w[C]_t = w[C]_0 \cdot \exp(-K_C \cdot t) \quad (1)$$

$$K_C = -\ln(w[C]_t / w[C]_0) / t \quad (2)$$

where $w[C]_0$ is the initial carbon content in the molten steel; $w[C]_t$ is the carbon content in the molten steel with time; K_C is apparent de-C rate constant (min^{-1}); t is de-C time (min).

For conventional process, the de-C reaction was divided into two stages: Stage-I (quick de-C period) and Stage-II (slow de-C period). In Stage-I, the K_{C1} value was high due to the high initial [C] content and $[O]_D$ content, which provided a high de-C reaction rate. Approximately 95% or more of the total [C] content was removed in this stage. When the [C] content dropped below 15×10^{-6}, the de-C changed to Stage-II. For CPA process, the de-C reaction was divided into four stages. In Stage-I (initial de-C period), the de-C rate was also high and the [C] content decreased from 233×10^{-6} to 100×10^{-6}. In Stage-II (stagnant de-C period), the K_{C2} value was approximately –0.53. The reasons for this phenomenon include: (1) vacuum level increased sharply due to the large amount of CO produced during the CPA process; (2) the oxygen in the vacuum vessel was consumed, and there was not enough oxygen to participate in the de-C reaction; (3) some carbon powder was dissolved in the molten steel during CPA. In Stage-III (quick de-C period), after the CPA, the de-C rate increased rapidly and the [C] content decreased from 165×10^{-6} to 13×10^{-6}, while the K_{C3} value curve for the CPA process and the K_{C1} value curve for the conventional process were parallel. Similarly to the conventional process, when the [C] content dropped below 15×10^{-6}, the de-C changed to the slow de-C period (Stage-IV).

Through the aforementioned analysis, compared to the conventional process, the de-C rate for the CPA process was lower, while the effect of CPA on the de-C rate was concentrated in the early period. However, due to the equilibrium [C] content being mainly determined by the CO partial pressure, the O activity in the molten steel (a[O]), and the

reaction ([C] + [O] = $CO_{(g)}$) equilibrium constant, the [C] content at the end of de-C in both processes presented a slight difference.

3.2. Behavior of [O] with CPA process

Fig. 7 shows the changes in $[O]_D$ concentration during RH de-C. Under the same initial conditions, the $[O]_D$ content at the end of de-C for CPA process was obviously lower than that for the conventional process. The $[O]_D$ content difference was 72×10^{-6}, when 50 kg of carbon powder were added at the [C]/[O] mass ratio of 0.37. The changes in $[O]_D$ content for the CPA process could be divided into three stages when compared to the conventional process. In Stage-I (0–3 min), the $[O]_D$ content was reduced by 100×10^{-6}–120×10^{-6} and the $[O]_D$ content change curve was consistent under the two different processes. In Stage-II (3–8 min), the $[O]_D$ content for the conventional process was higher compared to the CPA process. The $[O]_D$ content difference was 69×10^{-6} at the end of Stage-II. In Stage-III (8 min to end of de-C), as the de-C reaction occurred, the $[O]_D$ content continued to decrease; however, the reduction was not apparent. It could be observed from the [C] content change, as presented in section 3.1, that the [C] content dropped to about 50×10^{-6} when the de-C was at 8 min and the [C] reduction was very low. Consequently, the oxygen decrease was low.

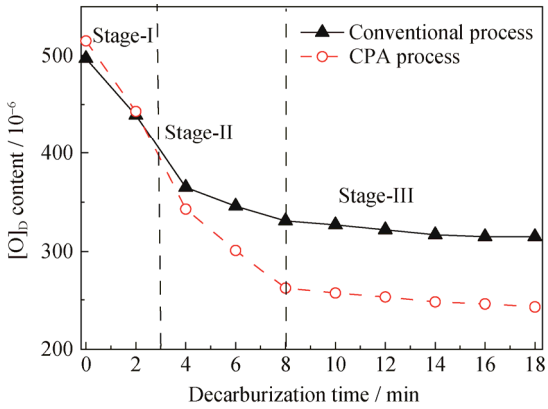

Fig. 7. Changes in $[O]_D$ content during RH de-C with CPA and conventional processes.

It could be observed from the latter analysis that the effect on the $[O]_D$ content for the CPA process was mainly concentrated in Stage-II (3–8 min). Following the CPA, carbon powder reacted with the $[O]_D$ quickly, achieving the goal of pre-deoxidation.

A higher $[O]_D$ content at the end of de-C might cause the over-oxidation of the molten steel. Therefore, in the ULC steel, the slag composition should be controlled to effectively improve the cleanliness of the molten steel. The $(CaO)/(Al_2O_3)$ mass ratio was controlled to within 1.2 and 2.0, while the sum content of FeO and MnO in the slag ((FeO + MnO)) was controlled low [12,22]. The slag compositions for different processes are shown in Fig. 8.

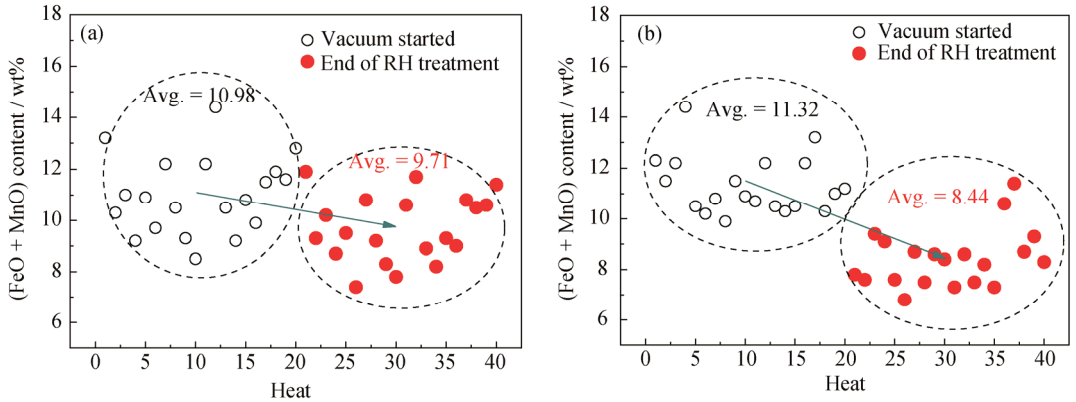

Fig. 8. (FeO+MnO) content changes in conventional process (a) and CPA process (b).

For conventional process, the (FeO + MnO) content decreased from 10.98wt% to 9.71wt%, for a decrease of 1.27wt%. Moreover, for the CPA process, the (FeO + MnO) content decreased from 11.32wt% to 8.44wt%, for a decrease of 2.88wt%. This indicated that the main difference in slag composition between the two processes was apparent in the decreased oxidation-capacity values. For the CPA process, the (FeO + MnO) content decreased by a higher margin, whereas the effect of reoxidation from the RH slag on the molten steel was lower. Therefore, the CPA process had the positive impacts on the $[O]_D$ reduction at the end of de-C as well as oxidation-slag reduction.

3.3. Modeling of de-C reaction in RH degasser

The mechanism of de-C in the RH degasser has been presented frequently in the literature. For the conventional process, the de-C mechanism is shown in Fig. 9(a), while the reactions were as follows [3,23–25]: (1) spontaneous CO bubbles formation within bulk steel; (2) reaction on Ar bubble surface; (3) reaction on molten steel surface.

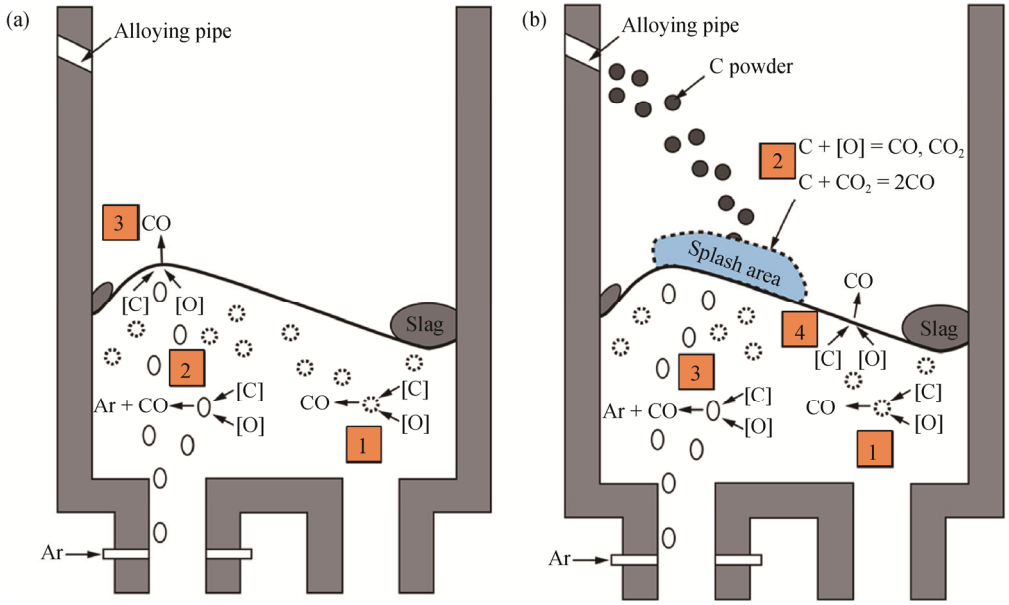

Fig. 9. Schematic drawing of reaction mechanisms of de-C in RH degasser: (a) conventional process; (b) CPA process.

For CPA process, the de-C mechanism changed. The change in appearance of the molten steel surface under the CPA process is presented in Fig. 10. When the pressure in the vessel was reduced to 2.25×10^4 Pa, the rapid evolution of CO bubbles was observed due to higher initial [C] and $[O]_D$ contents, while the evolution of CO bubbles was observed at the surface of the molten steel, as shown in Fig. 10(a). Fig. 10(b) presents the CPA process. Following CPA for 10 s, a violent reaction occurred on the molten steel surface and a severe splash occurred in the vacuum vessel, as shown in Fig. 10(c). The pre-deoxidization reaction was completed within 30 s, while the spatter was highly reduced, as shown in Fig. 10(d), and the appearance of the molten-steel surface was the same as before the CPA. When the [C] content decreased to 50×10^{-6}–100×10^{-6}, the CO evolution was only observed at the interface of the molten steel, as shown in Fig. 10(e), while the CO concentration started to drop quickly. When the [C] content was decreased to less than 50×10^{-6}, the CO evolution was hardly observed. Moreover, the molten steel surface became quiet, as shown in Fig. 10(f).

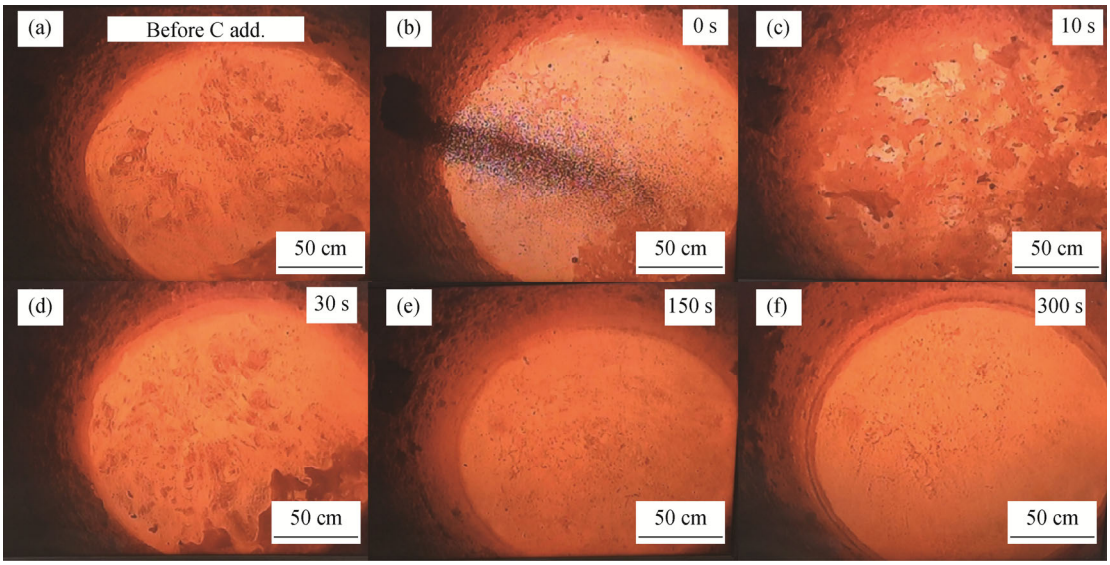

Fig. 10. Changes in appearance of molten steel surface under carbon addition: (a) 2.25×10^4 Pa, w[C] = 175×10^{-6}; (b) 2.5×10^4 Pa, w[C] = 100×10^{-6}; (c) 2.7×10^4 Pa, w[C] = 105×10^{-6}; (d) 3.0×10^4 Pa, w[C] = 126×10^{-6}; (e) 1.0×10^4 Pa, w[C] = 50×10^{-6}–100×10^{-6}; (f) 1×10^2 Pa, w[C] < 50×10^{-6}.

Therefore, the reaction mechanism of the de-C for the CPA process is described as shown in Fig. 9(b), while the reactions sites were as follows: (1) within the bulk steel, where the spontaneous CO bubbles form was the dominant

site in the beginning of RH process; (2) the main sites, where the de-C reaction occurred, were the splashing area on the liquid steel surface in the vacuum vessel; (3) Ar-bubble surface; (4) molten-steel surface. Following CPA, the C content increased sharply. The reaction of [C] and [O] in molten steel is limited due to the reaction of C powder and [O] in vacuum vessel, while the [C] content was no longer reduced as described in section 3.1. The mass transfer of [O] to the metal-gas surface was the limiting factor. Once the [C] content was lowered to 50×10^{-6}, the de-C reaction rate in the bulk steel was significantly decreased and the dominant reaction sites were Ar-bubble surface and molten-steel surface.

3.4. Aluminum consumption and total oxygen in steel

From the aforementioned analysis, it could be observed that for the CPA process, the $[O]_D$ content at the end of de-C and the RH slag reoxidation ability were significantly lower compared those with the conventional process. To further verify the effect of CPA on the cleanliness of the steel, $[O]_D$ content at the end of de-C and the aluminum consumption of 100 heats in the industrial production were compared. The results are shown in Fig. 11. Compared to the conventional process, the average content of $[O]_D$ at the end of de-C for the CPA process was decreased by 89×10^{-6}, while the aluminum consumption was decreased by 0.18 kg/t, and the defect rate of rolled products decreased from 2.2% to 1.3%. Therefore, the CPA process could not only reduce the aluminum consumption and cut the production costs, but also could significantly improve slab quality.

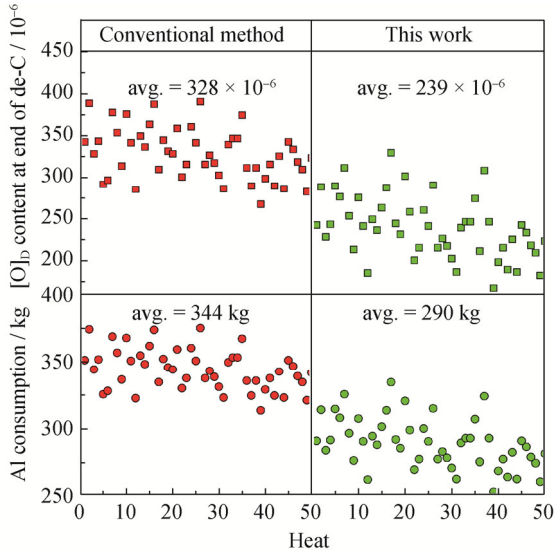

Fig. 11. Comparison of $[O]_D$ content at end of de-C and Al consumption for conventional and CPA processes.

4. Conclusions

In the present work, a pre-deoxidation method was adopted, adding carbon powder for ULC steel, to investigate and compare the [C] and [O] behavior in the RH degasser with the conventional process. The following conclusions could be drawn.

(1) For the CPA process, the change of [C] content was increased following the CPA. Following the addition of carbon powder for 1 min, the de-C reaction proceeded further. The de-C rate of the CPA process was lower compared to that of the conventional process, but the [C] content at the end of de-C was slightly different.

(2) The pre-deoxidation for the CPA process was completed within 5 min following CPA, whereas the CPA process could significantly reduce the $[O]_D$ content at the end of de-C as well as the (FeO + MnO) content.

(3) For the CPA process, spontaneous CO-bubbles formation within bulk steel was the dominant mechanism at the beginning of the RH process; with CPA, the main de-C site was the splashing area on the liquid-steel surface in the vacuum vessel; when the content of [C] dropped below 50×10^{-6}, the bath and bubble surfaces were the major sites of de-C.

(4) The industrial production data demonstrated that the CPA process could reduce $[O]_D$ at the end of RH by 89×10^{-6} and aluminum consumption by 0.18 kg/t, the defect rate of rolled products decreased from 2.2% to 1.3%, CPA was beneficial in improving ULC steel cleanliness.

Acknowledgements

This study was financially supported by the National Natural Science Foundation of China (No. 51874021), Fundamental Research Funds for the Central Universities of China (No. FRF-IC-18-002) and State Key Laboratory of Advanced Metallurgy Foundation of China (No. 41618019). The authors are thankful to Magang (Group) Holding Co., Ltd. for the support on the field test.

References

[1] M. Takahashi, H. Matsumoto, and T. Saito, Mechanism of de-C in RH degasser, *ISIJ Int.*, 35(1995), No. 12, p. 1452.

[2] G.J. Chen and S.P. He, Circulation flow rate and de-C in the RH degasser under low atmospheric pressure, *Vacuum*, 153(2018), p. 132.

[3] Y.H. Li, Y.P. Bao, R. Wang, L.F. Ma, and J.S. Liu, Modeling study on the flow patterns of gas–liquid flow for fast de-C during the RH process, *Int. J. Miner. Metall. Mater.*, 25(2018),

No. 2, p. 153.

[4] J. Guo, S.S. Cheng, H.J. Guo, and Y.G. Mei. Novel mechanism for the modification of Al_2O_3-based inclusions in ultra-low carbon Al-killed steel considering the effects of magnesium and calcium, *Int. J. Miner. Metall. Mater*, 25(2018), No. 3, p. 280.

[5] M. Wang, Y.P. Bao, Q. Yang, L.H. Zhao, and L. Lin, Coordinated control of carbon and oxygen for ultra-low-carbon interstitial-free steel in a smelting process, *Int. J. Miner. Metall. Mater.*, 22(2015), No. 12, p. 1252.

[6] D.Q. Geng, J.X. Zheng, K. Wang, P. Wang, R.Q. Liang, H.T. Liu, H. Lei, and J.C. He, Simulation on de-C and inclusion removal process in the ruhrstahl-heraeus (RH) process with ladle bottom blowing, *Metall. Mater. Trans. B*, 46(2015), No. 3, p. 1484.

[7] Y.H. Li, Y.P. Bao, R. Wang, M. Min, Q.X. Huang, and Y.G. Li, Modeling of liquid level and bubble behavior in vacuum chamber of RH process, *J. Iron. Steel Res. Int.*, 23(2016), No. 4, p. 305.

[8] T. Kuwabara, K. Umezawa, K. Mori, and H. Watanabe, Investigation of decarburization behavior in RH-reactor and its operation improvement, *Trans. Iron Steel Inst. Jpn.*, 28(1988), No. 4, p. 305.

[9] B.K. Li and T. Fumitaka, Modeling of circulating flow in RH degassing vessel water model designed for two-and multi-legs operations, *ISIJ Int*., 40(2000), No. 12, p. 1203.

[10] G.J. Chen and S.P. He, Mixing behavior in the RH degasser with bottom gas injection, *Vacuum*, 130(2016), p. 48.

[11] H. Takechi, Metallurgical aspects on interstitial free sheet steel from industrial viewpoints, *ISIJ Int.*, 34(1994), No. 1, p. 1.

[12] Y.M. Qin, X.H. Wang, L.P. Li, and F.X. Huang, Effect of oxidizing slag on cleanliness of IF steel during ladle holding process, *Steel Res. Int*., 86(2015), No. 9, p. 1037.

[13] E. Zinngrebe, C. Van Hoek, H. Visser, A. Westendorp, and I.H. Jung, Inclusion population evolution in Ti-alloyed Al-killed steel during secondary steelmaking process, *ISIJ Int.*, 52(2012), No. 1, p. 52.

[14] F. Zhang and G.Q. Li, Control of ultra low titanium in ultra low carbon Al-Si killed steel, *J. Iron Steel Res. Int*., 20(2013), No. 4, p. 20.

[15] G.H. Li, B. Wang, Q. Liu, X.Z. Tian, R. Zhu, L.N. Hu, and G.G. Cheng, A process model for BOF process based on bath mixing degree, *Int. J. Miner. Metall. Mater.*, 17(2010), No. 6, p. 715.

[16] P.H. Li, Y.P. Bao, F. Yue, and J. Huang, BOF end-point control of ultra low carbon steel, *Iron Steel*, 46(2011), No. 10, p. 27.

[17] N. Jia, Y.B, Zhang, and M.W. Wu, Deoxidation practice with high-quality carbon powder to substitute part of Ferro-Aluminum in tapping of converter, *Hebei Metall.*, 237(2015), No. 9, p. 56.

[18] J.L. Guo, Y.P. Bao, and M. Wang, Cleanliness of Ti-bearing Al-killed ultra-low-carbon steel during different heating processes, *Int. J. Miner. Metall. Mater.*, 24(2017), No. 12, p. 1370.

[19] Y. Kishimoto, K. Yamaguchi, T. Sakuraya, and T. Fujii, De-C reaction in ultra-low carbon iron melt under reduced pressure, *ISIJ Int.*, 33(1993), No. 3, p. 791.

[20] S. Inoue, Y. Furuno, T. Usui, and S. Miyahara, Acceleration of de-C in RH vacuum degassing process, *ISIJ Int.*, 32(1992), No. 1, p. 120.

[21] B.S. Liu, G.S. Zhu, H.X. Li, B.H. Li, and A.M. Cui, De-C rate of RH refining for ultra low carbon steel, *Int. J. Miner. Metall. Mater.*, 17(2010), No, 1, p. 22.

[22] C.Y. Liu, F.X. Huang, and X.H. Wang, The effect of refining slag and refractory on inclusion transformation in extra low oxygen steels, *Metall. Mater. Trans. B*, 47(2016), No. 2, p. 999.

[23] M.A. van Ende, Y.M. Kim, M.K. Cho, J. Choi, and I.H. Jung, A kinetic model for the Ruhrstahl Heraeus (RH) degassing process, *Metall. Mater. Trans. B*, 42(2011), No. 3, p. 477.

[24] Y. Higuchi, H. Ikenaga, and Y. Shirota, Effects of [C], [O] and pressure on RH vacuum de-C, *Tetsu-to-Hagané*, 84(1998), No. 10, p. 709.

[25] Y.G. Park and K.W. Yi, A new numerical model for predicting carbon concentration during RH degassing treatment, *ISIJ Int.*, 43(2007), No. 9, p. 1403.